AIAA JOURNAL
Vol. 32, No. 9, September 1994

Velocity Measurements in Turbulent Bluff-Body Stabilized Flows

R. W. Schefer*
Sandia National Laboratories, Livermore, California 94550
and
M. Namazian† and J. Kelly‡
Altex Technologies Corporation, Santa Clara, California 95054

Velocity measurements have been obtained in a turbulent bluff-body stabilized flow. The flow configuration consisted of a 5.4-mm-diam methane jet separated from an outer, annular air flow by a 50-mm-diam bluff body. Results were obtained for three fuel-jet to outer air velocity ratios to study the effects of inlet velocity ratio on the turbulence and flowfield characteristics. At low inlet velocity ratios the flow can best be described as dominated by the reverse flow of the annular air stream and exhibits well-defined fuel jet and annular air stagnation points along the centerline. As the velocity ratio is increased, fuel-jet penetration increases until the dynamic pressure of the jet is sufficient to overcome the adverse pressure gradient of the outer air, and the fuel jet penetrates the recirculation zone. Under these conditions the stagnation points move off the centerline, and the flow is best described as dominated by the fuel jet. Probability distributions of individual velocity components are bimodal in regions of high shear located along the recirculation zone boundaries and in downstream stagnation zones. Conditional seeding of the central jet and annular air shows that the two modes of the bimodal distributions are associated with the alternate passage of unmixed fuel and air through the measurement volume. The observed data are interpreted in terms of instantaneous Mie scattering pictures, which emphasize the importance of large-scale structure and intermittency in these flows.

I. Introduction

NONPREMIXED bluff-body stabilized flows provide a useful research tool for the study of turbulence and mixing in elliptic flows. Recirculating flow geometries, in which recirculation is typically induced by a solid body (i.e., baffle, cone, or bluff body) or by swirl introduced at the inlet, form the basis for a number of practical combustion devices in which the recirculation of high temperature combustion products provides improved flame stabilization and combustion characteristics relative to jet flows with no recirculation. The importance of recirculating flows in practical combustion devices has resulted in considerable interest in the development of numerical models for these flows.

Computational models for both isothermal and reacting bluff-body flows have been previously developed. In general, the application of conventional time-averaged approaches using k-ε turbulence models to predict isothermal bluff-body flows has met with limited success.[1-4] Comparisons with limited experimental measurements showed that although qualitative flow features (mean concentration and velocity field, stagnation point locations) were predicted, turbulence quantities such as fluctuation intensities and turbulent kinetic energy were significantly underpredicted. In particular, discrepancies between predicted and experimental results increased for higher jet velocities where observations indicated that the flow becomes more "unsteady" and organized large-scale structure may dominate the flow.[4,5]

Increasing evidence exists for the importance of unsteady, and perhaps periodic, large-scale structure in bluff-body flows. Based on the analogy between bluff-body and swirl stabilized flowfields, it appears likely that such a structure may also be important in a wide variety of recirculating flows. Some evidence for this comes from the studies carried out in bluff-body stabilized flames at the Air Force Aeronautical Propulsion Laboratory using propane as the fuel.[6,7] Flame emission and velocity measurements clearly revealed the periodic expulsion of flame slugs, or "turbules," from the recirculation zone, which were subsequently convected downstream.[8] Studies by the present authors using species concentration imaging techniques also conclude that flow and mixing is dominated by large-scale structure.[9]

The limited available comparisons between experimental measurements and time-averaged models leave the limitations of these models and the extent to which they can be applied to recirculating flows uncertain. Clearly more data in well-defined flows is needed to fully evaluate model approaches. In addition, given the potential importance of periodic large-scale structure, the role and presence of large-scale structure must be experimentally established, particularly the relationship between this structure and quantitative point statistics. Toward this objective, planar CH_4 imaging data were reported previously by the present authors for a concentric jet of CH_4 and air separated by a bluff body.[9] Several jet-to-air velocity ratios were studied under isothermal conditions. The jet-to-air velocity was found to be an important parameter in determining the flow characteristics, particularly mixing between the fuel and air.

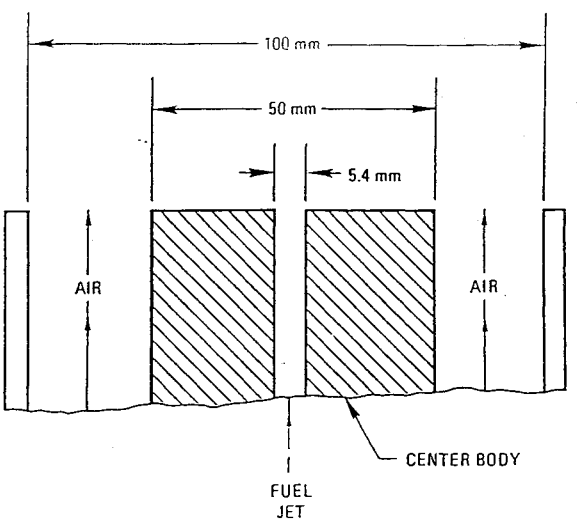

Fig. 1 Schematic of experimental apparatus.

Received Oct. 1, 1992; revision received Jan. 28, 1994; accepted for publication Feb. 5, 1994.

*Senior Member Technical Staff, Combustion Research Facility.
†Vice President, 650 Nuttman Road.
‡President, 650 Nuttman Road.

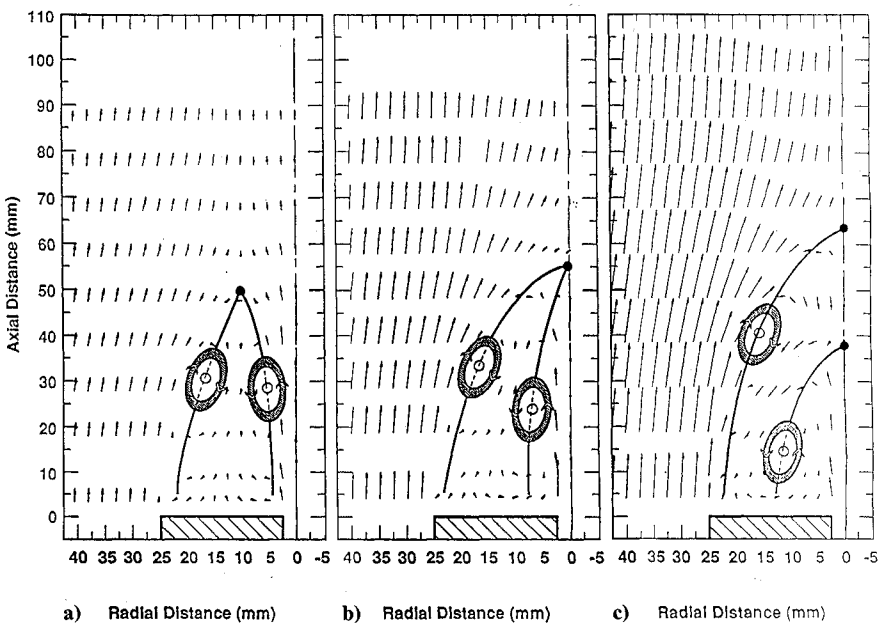

Fig. 2 Measured velocity vectors in a bluff-body stabilized methane jet: a) $U_j/U_a = 2.8$, b) $U_j/U_a = 1.4$, and c) $U_j/U_a = 0.84$.

Velocity measurements have been obtained in the present investigation using two-color laser Doppler velocimetry at the same inlet flow conditions as this earlier study. The objective of the measurement is to supplement the previous CH_4 concentration data and to provide quantitative information on important turbulence quantities related to turbulent mixing. Because of the importance of large-scale flow structure, the data will be presented in a form that identifies the relationship of the velocity statistics to the large-scale flow structure. In the remainder of this paper the experimental system will be described, and the experimental results will be presented. Axial and radial profiles of single-point velocity statistics will be described first. Next, the probability distributions of the axial and radial velocity will be presented and used to interpret the measured variations in axial and radial velocity with flowfield location. Finally, conditional seeding measurements will be described to better understand the source of the high turbulence intensities measured and the resulting implications for modeling these flows.

II. Experimental

Figure 1 shows a schematic of the axisymmetric bluff-body burner. Methane fuel was supplied through the center of the bluff body at a velocity U_j of 21 m/s corresponding to a Reynolds number Re_j based on the 5.4-mm fuel-jet diameter d_f of 7000. Velocity measurements at the jet exit showed that the maximum velocity at the centerline ($u_{j,\max} = 26$ m/s) was consistent with fully developed, turbulent pipe flow ($u_{j,\max}/u_{\text{avg}} = 1.28$). Air was supplied through a coaxial jet surrounding the bluff body at velocities U_a of 7.5, 15, and 25 m/s resulting in jet-to-air velocity ratios U_j/U_a of 2.8, 1.4, and 0.84. The measured velocity profile across the annular inlet section for the air was uniform to within 1%, with a turbulence level of less than 0.7% rms. Based on the bluff-body diameter D_b of 5 cm and the inlet air velocity, the maximum air Reynolds number Re_a was 1.1×10^5.

The laser Doppler velocimetry (LDV) system is described in detail elsewhere.[10] The LDV measurements were made with a two-color, dual-beam, real-fringe system. With this system the axial velocity u and either the radial v or azimuthal velocity w could be measured simultaneously. The second component was selected by measuring the radial profiles along one of two perpendicularly oriented radial lines so as to properly orient the LDV fringes for measuring the desired component.

The data were analyzed to obtain mean and fluctuating velocities and the corresponding probability density distributions. Radial profiles were obtained at 12 axial stations located up to 140 mm downstream of the burner surface. Each radial profile consisted of 20 equally spaced locations with 2.5-mm separation between measurement locations. Typically 5000 velocity measurements were obtained at each spatial location, whereas up to 20,000 measurements were taken at locations where higher order statistics were calculated. The estimated uncertainties in the velocity statistics, determined from repeated data sets (consisting of 5000 measurements each) and from initial system calibration data, are as follows: $\bar{u} = \pm 1\% \ldots \bar{v} = \pm 3\%$, $(\overline{u'^2})^{1/2} = \pm 3\% \ldots (\overline{v'^2})^{1/2} = \pm 3\%$, and $\overline{u'v'} = \pm 5\%$.

Additional information on mixing between the fuel jet and annular air was obtained by alternately adding LDV seed particles only to the fuel jet and only to the annular air. The conditional statistics measured by this seeding technique provide an indication of the extent to which fluid originating from two initially separate inlet streams has mixed. That is, statistics conditional on fluid originating from the annular air consist of contributions from 1) unmixed air and 2) air which has previously been entrained and subsequently mixed with jet fluid. Similarly, statistics conditional on fluid originating from the jet consist of contributions from 1) unmixed jet fluid and 2) jet fluid that has been mixed with entrained air.

III. Results

A. General Flowfield Characteristics

Velocity vector plots of the mean velocity in a plane through the burner axis are shown in Fig. 2 for $U_j/U_a = 2.8$, 1.4, and 0.84. At the highest U_j/U_a ratio of 2.8 (Fig. 2a) the flow along the axis resembles a free-jet case. The external air flow, after emerging from the annular jet, converges toward the axis and merges with the fuel jet at an axial distance x of approximately 55 mm. Between the converging air flow and the fuel jet are two counter-rotating eddies. The eddy centers and rotational directions are highlighted in the figure. The eddies are associated with the fuel and air jets, rotate counterclockwise and clockwise, respectively, and are centered at about the same axial location. The zero axial velocity lines, separating upstream from downstream flowing gases, are also indicated. The $U_j/U_a = 2.8$ case is an example of a penetrating jet in which the fuel jet penetrates the downstream end of the recirculation zone. Although no centerline stagnation points exist, a stagnation point is located at a radial location of about 10 mm from the centerline where the zero axial velocity lines converge.

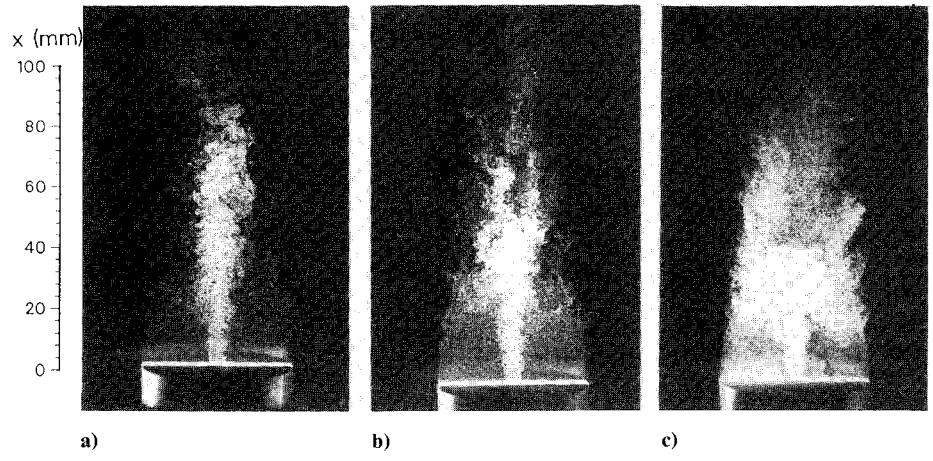

Fig. 3 Two-dimensional Mie scattering measurements of the instantaneous particle distribution in a bluff-body stabilized methane jet; the scattering particles have been added to the fuel stream: a) $U_j/U_a = 2.8$, b) $U_j/U_a = 1.4$, and c) $U_j/U_a = 0.84$.

As the inlet air velocity is increased ($U_j/U_a = 1.4$ in Fig. 2b), the fuel and air eddies shift upstream and downstream, respectively. Most significantly, a single stagnation point is formed along the centerline at an axial location of about $x = 60$ mm. This is the lowest air velocity at which stagnation of the fuel jet occurs and is termed the incipient nonpenetrating-jet case. Further increases in the inlet air velocity ($U_j/U_a = 0.84$ in Fig. 2c) result in upstream movement of the fuel-jet stagnation point toward the jet exit. A second stagnation point, termed the air stagnation point, is also formed farther downstream along the centerline at $x = 65$ mm. The air stagnation point location is controlled mainly by the bluff-body diameter and does not vary significantly with U_j/U_a. For the $U_j/U_a = 0.84$ case, the eddy centers are farther displaced from each other, and the region of the flow between the zero axial velocity streamlines is greater than in the higher velocity ratio cases.

The dynamics of recirculating flows of this type can be understood in terms of the pressure balance established between the central jet and annular air. As the air flow converges toward the centerline, the static pressure increases. The degree to which the fuel jet penetrates the recirculation zone is associated with the distribution of dynamic pressure across the fuel jet relative to the dynamic pressure created by the recirculating air flow. The jet loses dynamic pressure with distance from the exit due to the entrainment of ambient fluid. Therefore, as air velocity and thereby stagnation pressure increases, the fuel jet stagnates closer to the jet exit to maintain a balance between the available jet dynamic pressure and the air stagnation pressure. For low fuel-to-air velocity ratios, jet dynamic pressure is insufficient to overcome the air flow, and the jet stagnates farther upstream. As the fuel-jet velocity is increased, the fuel-jet penetration distance increases before entrainment reduces the dynamic pressure to the level where it balances the air flow. At higher fuel-to-air velocity ratios, portions of the jet near the axis will have enough dynamic pressure to overcome the static pressure produced by the air flow and will penetrate along the axis. However, portions of the jet farther away from the axis will not have sufficient dynamic pressure and will be turned back upstream, resulting in the off-axis stagnation point seen in Fig. 2a for $U_j/U_a = 2.8$.

It is important to note that the instantaneous flow structure differs considerably from the time-averaged behavior presented in Fig. 3. This difference can be seen from the Mie scattering photographs shown in Fig. 3 where small diameter alumina particles have been added to the fuel jet.[11] Here the short, 8-ns pulse duration of the illuminating laser effectively freezes the particle motion and provides an indication of the instantaneous flow structure. The higher intensity region near the jet centerline identifies the higher seed region associated with the fuel jet. The recirculation patterns observed in Fig. 2 are a time-averaged result and rarely appear instantaneously. In addition, the smooth transition from high to lower velocities across the shear layers adjacent to both the fuel jet and along the outer recirculation zone boundaries actually is quite irregular and indicative of larger scale structure that forms in regions of higher shear. Particularly apparent in Fig. 3a is the growth of periodic rollup-type structures in the outer air shear layer, which is related to vortex shedding from the outer edges of the bluff-body surface. Also apparent in this figure are large regions devoid of particles, indicating that large-scale transport is significant.

B. Mean and Fluctuating Velocities

1. Axial Profiles

Profiles of the mean and fluctuating velocity statistics provide a more detailed look at the flowfield characteristics. Results along the axis are particularly helpful in defining the nature of the stagnation region. Figure 4 shows the mean axial $\bar{u}$ and fluctuating (rms) axial and radial velocities $\overline{u'}$ and $\overline{v'}$ as a function of axial distance for $U_j/U_a = 2.8$, 1.4, and 0.84. Also shown is a 0-m/s air velocity case ($U_j/U_a = \infty$), representing a turbulent jet into ambient air.

Figure 4a shows the typical $1/x$ centerline decay rate of mean axial velocity for the turbulent jet into ambient air. Initially there is a nearly constant velocity zone that is associated with the potential core region. In this initial zone, the fluctuating velocity components are small. However, once the developing shear layers located on both sides of the jet merge along the axis, fluctuations quickly reach a peak at about $x = 30$ mm. As the mean velocity decays, the fluctuations also begin to decay. Since the radial and axial fluctuating components are nearly equal in magnitude, the turbulence in this flow is close to isotropic.

For $U_j/U_a = 2.8$, the initial part of the axial velocity decay is similar to the turbulent jet. However, at approximately 45 mm the velocity drops more steeply than in the jet, and at about 80 mm the velocity goes through a minimum and begins to rise. From Fig. 2a, the 45-mm location corresponds to the merging of the fuel jet and annular air. At this location the pressure increases and, thereby, the velocity decreases. The 80-mm location is approximately where the velocities are nearly parallel to the axis. Beyond this location, the flow takes on a wake-like character and the axial velocity is expected to recover to the initial air velocity of 7.5 m/s. In contrast to the jet results, two peaks are observed in $\overline{u'}$ along the centerline. The first, at about 25 mm, is higher than the maximum in the jet profile and is shifted farther upstream. The second peak, more apparent as a flat region, occurs near the downstream end of the recirculation zone. Similar but less obvious peaks can be observed in the fluctuating radial velocity.

Increasing the air velocity to $U_j/U_a = 1.4$ causes the flow to stagnate along the axis at approximately 55 mm. The initial velocity

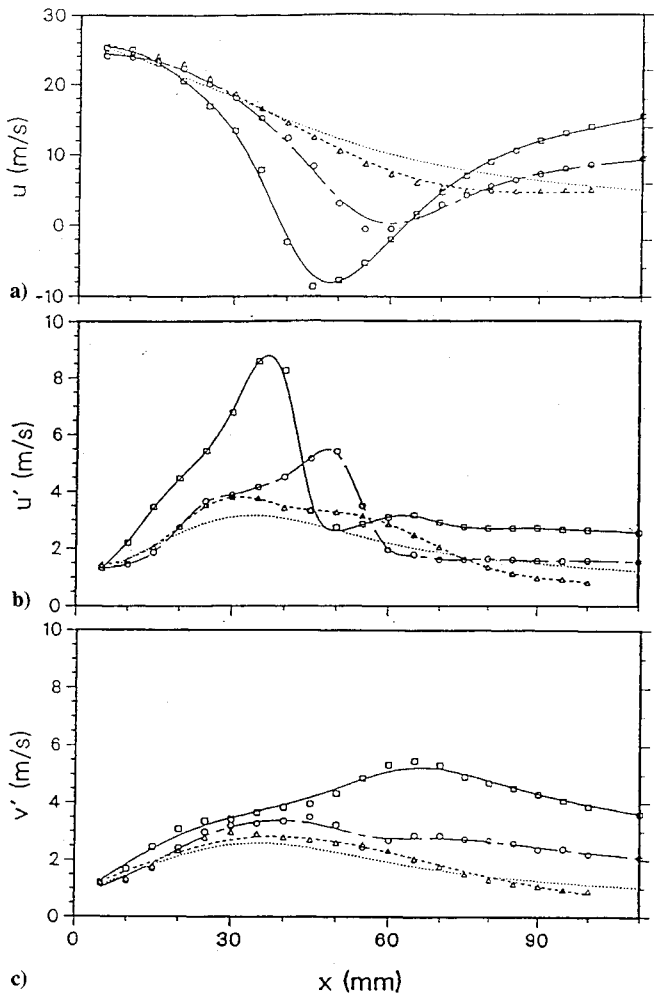

Fig. 4 Centerline variation in mean and fluctuating axial and radial velocities in bluff-body stabilized methane jet: U_j/U_a = 2.8, Δ; U_j/U_a = 1.4, ○; U_j/U_a = 0.84, □; and dotted line represents data for a methane jet into ambient air (jet velocity = 21 m/s).

fluctuation levels are consistent with the U_j/U_a = 2.8 case. However, at approximately 50 mm, the fluctuating axial velocity component is sharply peaked and comparable to the mean velocity value. Planar imaging measurements of the instantaneous CH_4 distribution show that the stagnation point location is characterized by large-scale concentration fluctuations.[9] These fluctuations are driven by large-scale intermittent movement of the fuel/air interface through this location. Since the fuel and air sides of the boundaries are characterized by downstream and upstream flowing fluid, respectively, the velocity fluctuations can be large even though the mean velocity is relatively small. From approximately 20 to 100 mm, the turbulence is highly nonisotropic relative to a jet.

At a velocity ratio of U_j/U_a = 0.84, the axial velocity is zero at x = 40 and 65 mm, corresponding to separate fuel and air stagnation points along the axis. The axial fluctuations peak at the fuel stagnation point, and the radial fluctuations peak at the air stagnation point. Secondary peaks for the fluctuating axial and radial velocities can also be seen at the air and fuel stagnation points, respectively. Both the axial and radial fluctuations are large compared to the mean velocity at their respective stagnation points. Once again, the turbulence is highly nonisotropic at these locations.

The fuel and air stagnation points can be characterized as classical stagnation flows oriented along and perpendicular to the centerline, respectively. For the fuel stagnation point, the flows are opposed along the axis, and axial fluctuations are maximized for this case. For the air stagnation point, the flows are opposed perpendicular to the axis, which maximizes the radial fluctuations. The large fluctuations in the location of these stagnation zones and the resulting high velocity fluctuations are a result of the passage of large-scale interfaces separating fuel and air through the sampling volume. The conditionally seeded and probability density function velocity results described subsequently support this hypothesis.

2. *Radial Profiles*

Radial variations in the mean and fluctuating velocities are shown in Figs. 5–7 for axial locations of x = 30, 50, and 70 mm, respectively. For all three velocity ratios an axial location of x = 30 mm corresponds to the central recirculation zone, x = 50 mm is just upstream of the air stagnation zone, and x = 70 mm is downstream of the air stagnation zone where the fuel jet and annular air have merged into a wake-like flow region. The development of the velocity field is similar at each axial location. The negative values of $\bar{u}$ at upstream locations clearly indicate the location and radial extent of the recirculation zone. The mean radial velocity profiles show outward flow of the central jet fluid (positive values) and inward flow (negative values) of annular air converging toward the centerline. The axial and radial fluctuations attain their maximum values in regions where the mean velocity gradients are high. These regions include the shear layers located along the central jet and outer recirculation zone boundaries and in the stagnation zone. The correlation between velocity components $\overline{u'v'}$ is also highest in the shear regions. Inside the recirculation zone the mean and fluctuating velocity distributions are relatively uniform.

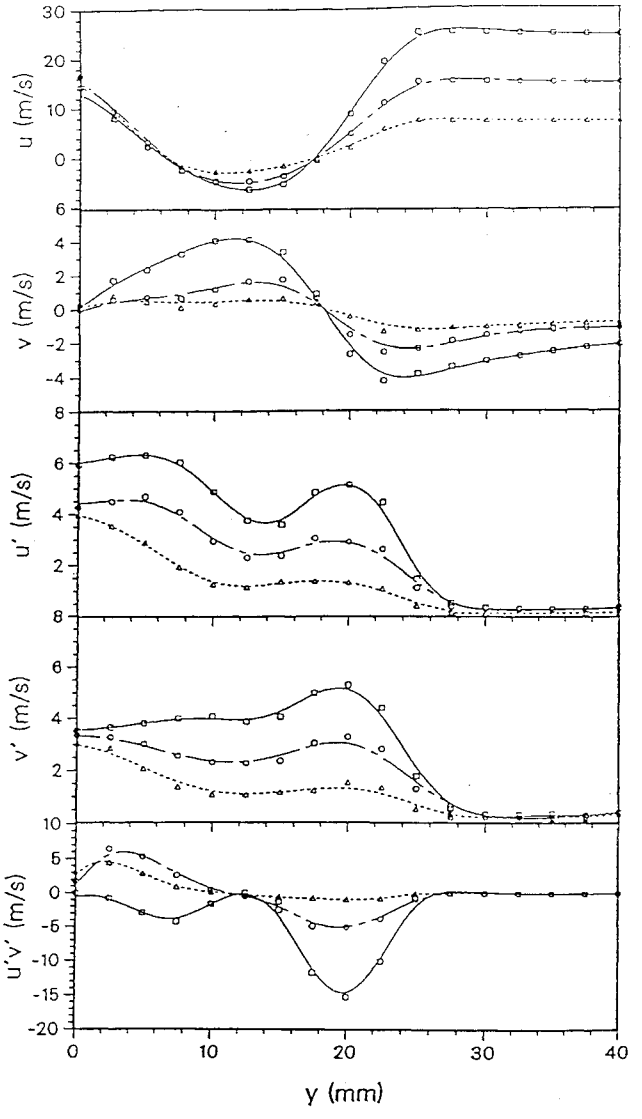

Fig. 5 Radial variation in mean and fluctuating axial and radial velocities and their correlation in bluff-body stabilized methane jet, axial location x = 30 mm: U_j/U_a = 2.8, Δ; U_j/U_a = 1.4, ○; and U_j/U_a = 0.84, □.

C. Probability Density Distributions

Probability distributions for the axial and radial velocity were calculated from up to 20,000 measurements at each spatial location. Typically, the distributions are unimodal and nearly Gaussian at all locations with the exceptions of the centerline stagnation regions and the shear layers located adjacent to the central jet and along the outer edge of the recirculation zone, where the distributions are bimodal. Figure 8 presents probability distributions at several locations along the centerline for the air dominated case ($U_j/U_a = 0.84$). Both the axial $P(u)$ and radial $P(v)$ velocity distributions are given. As noted earlier, the 40-mm location corresponds to the fuel-jet stagnation zone where axial velocity fluctuations are maximum whereas the 65-mm location corresponds to the air stagnation point where the radial fluctuations are highest. Figure 8 shows that $P(u)$ is bimodal at 40 mm whereas $P(v)$ is nearly Gaussian. The bimodal axial velocity distribution consists of two major contributions associated with upstream ($u < 0$) and downstream ($u > 0$) flowing fluid. The conditionally seeded results presented in the following section show that the upstream flow is primarily air originating from the air stagnation zone and the downstream flow is fuel from the central jet. Moving downstream through the fuel stagnation region shows that the most probable mode shifts from that associated with the jet fluid ($u > 0$) to that associated with the air ($u < 0$). Upstream and downstream of the fuel stagnation point the distributions are unimodal and overlap with the fuel or air parts of the adjacent bimodal distributions, respectively. At the air stagnation point ($x = 65$ mm), $P(u)$ is nearly Gaussian whereas $P(v)$ is bimodal, which accounts for the high radial velocity fluctuations at this location.

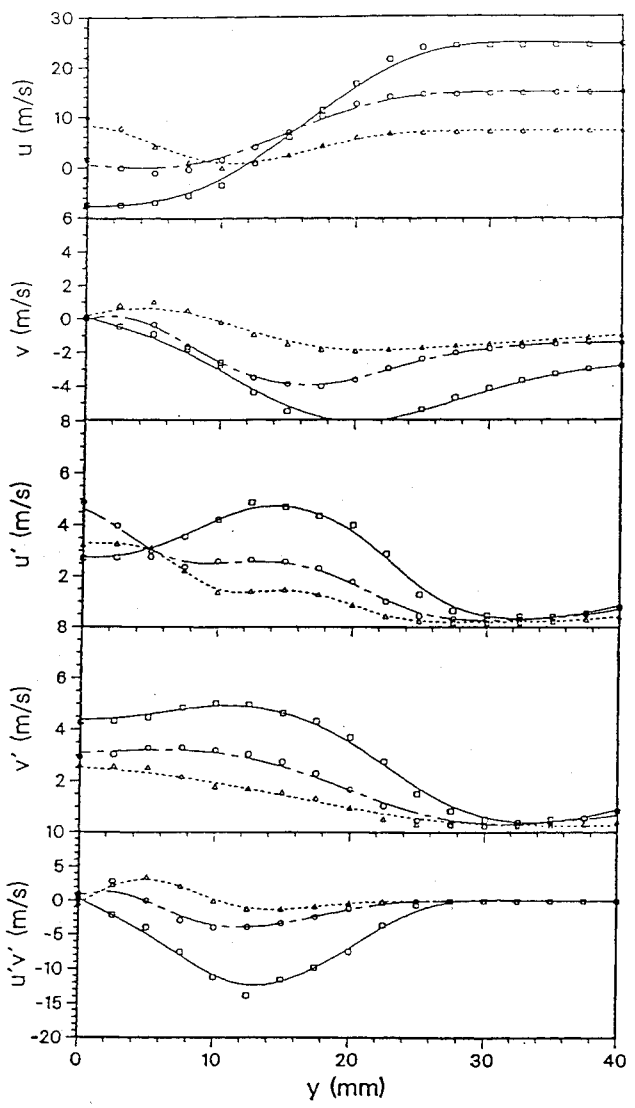

Fig. 6 Radial variation in mean and fluctuating axial and radial velocities and their correlation in bluff-body stabilized methane jet, axial location x = 50 mm: U_j/U_a = 2.8, Δ; U_j/U_a = 1.4, ○; and U_j/U_a = 0.84, □.

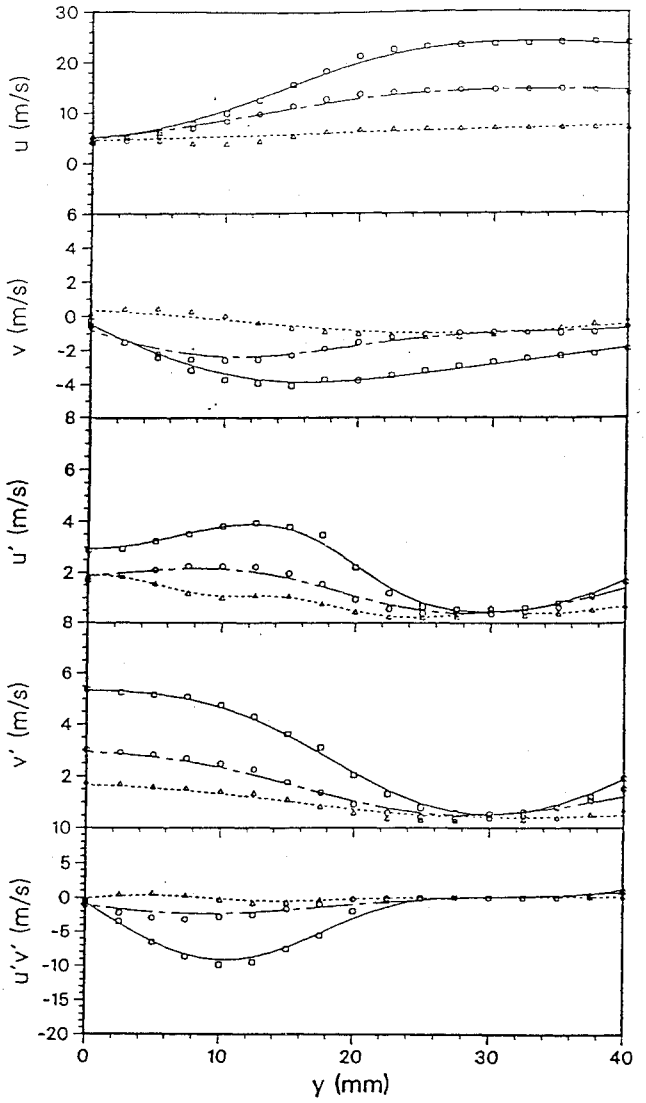

Fig. 7 Radial variation in mean and fluctuating axial and radial velocities and their correlation in bluff-body stabilized methane jet, axial location x = 70 mm: U_j/U_a = 2.8, Δ; U_j/U_a = 1.4, ○; and U_j/U_a = 0.84, □.

Shown in Fig. 9 are the bimodal probability distributions corresponding to the outer shear layer located between the annular air and the recirculation zone ($y = 17.5$ mm) and the shear layer adjacent to the central jet ($y = 7.5$ mm). Both $P(u)$ and $P(v)$ are bimodal in the outer shear layer, whereas only $P(u)$ is bimodal adjacent to the central jet. In both shear layers, the axial velocity distributions show positive and negative peaks. The negative peak is associated with upstream flowing recirculation zone fluid whereas the positive peaks represent the contributions of downstream flowing annular air in the outer shear layer and downstream flowing jet fluid adjacent to the central jet. Similar results (not shown) were obtained for inlet velocities ratios of U_j/U_a = 1.4 and 0.84, with bimodal velocity distributions observed in the shear layers and in the stagnation zone where the velocity fluctuations are highest.

D. Conditional Measurements

Conditional velocity measurements, in which LDV seed particles were added only to the fuel jet or only to the annular air, were made to better understand the source of the high fluctuations and the bimodal velocity distributions. The resulting velocity measure-

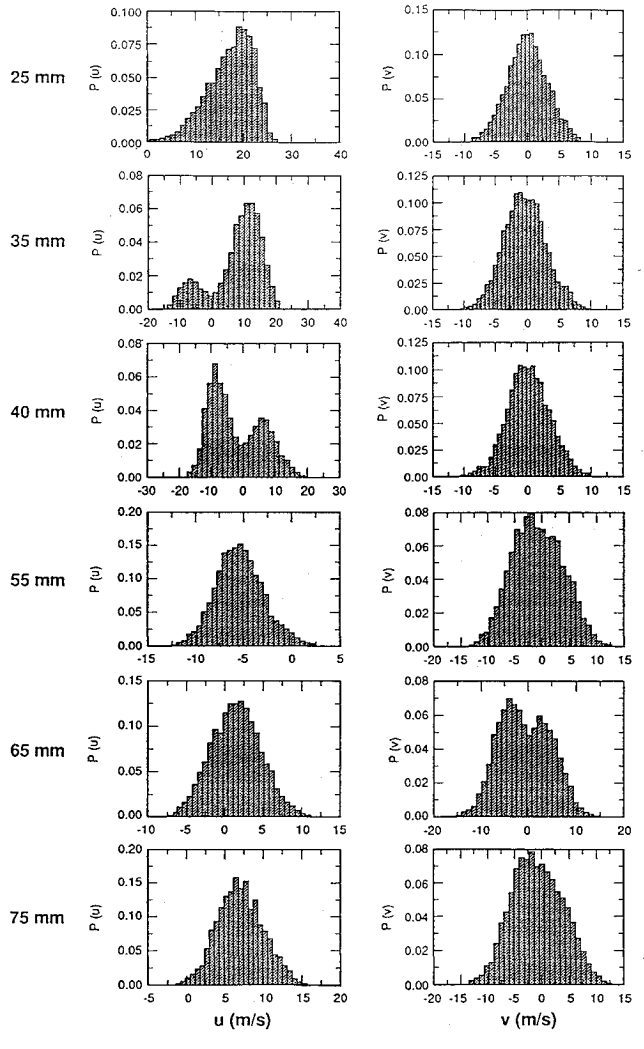

Fig. 8 Probability distributions of axial (left) and radial (right) velocity in a bluff-body stabilized methane jet; distributions are shown for various axial locations along the centerline, $U_j/U_a = 0.84$.

ments are conditional on fluid originating from either the fuel jet (denoted by the subscript j) or the annular air (subscript a). As discussed earlier, this conditional seeding provides information on the degree of turbulent mixing, since the seed particles provide a marker for fluid originating from the two initially separated inlet flows.

Conditionally sampled probability density distributions of axial and radial velocity along the centerline for $U_j/U_a = 0.84$ are shown in Fig. 10. Distributions are shown at the fuel stagnation point (Fig. 10a) where the axial velocity distribution is bimodal and at the air stagnation point (Fig. 10b) where the radial velocity distribution is bimodal. Comparison of the distributions conditional on the jet fluid $P(u)_j$ and on the air $P(u)_a$ at the fuel stagnation point clearly shows that the positive velocity peak at +10 m/s is primarily associated with downstream flowing jet fluid whereas the negative peak at −10 m/s is associated with upstream moving air. The large difference between $P(u)_j$ and $P(u)_a$ is indicative of the small amount of mixing between the two fluids at this location and can best be interpreted as axial oscillations in the location of the instantaneous stagnation point.

The conditional radial velocity distributions $P(v)_j$ and $P(v)_a$ at the air stagnation point (Fig. 10b) do not show significant differences and are quite similar to the conventionally average distribution in Fig. 8. This similarity indicates that fluid originating from the fuel jet and the annular air has undergone significant mixing prior to reaching the air stagnation region. The bimodal distributions with both positive and negative peak values further indicate a periodic motion perpendicular to the centerline with the dominant direction alternately to the right and to the left. Considering the previous description of the air stagnation point as a classical stagnation flow oriented perpendicular to the centerline, oscillations in the radial location of the stagnation point are consistent with this behavior.

Similar conditional seeding measurements in the outer shear layer show that the positive peak in $P(u)$ at $y = 17.5$ mm (see Fig. 9) corresponds to annular air flowing in the downstream direction, whereas the negative peak corresponds to mixed fluid flowing upstream as part of the recirculation zone. The alternate presence of annular air and recirculation zone fluid in the measurement volume is indicative of a radially oscillating boundary between the air and recirculation zone, probably due to the interaction between this boundary and periodic vortex shedding from the bluff body as seen in the Mie scattering images of Fig. 3. In the central jet shear layer, the positive peak is primarily jet fluid with some entrained air flowing downstream, whereas the negative peak is again mixed recirculation zone fluid.

In summary, it can be concluded that the velocity in the vicinity of the stagnation zone consists of alternate contributions from fuel and air that have substantially different velocities. These contributions create the bimodal distributions that, when time averaged, lead to the very high fluctuations indicated in the stagnation zone. Similarly, fluctuations in the recirculation zone shear layers consist of alternate contributions from recirculation zone fluid and either the annular air (outer shear layer) or central jet fluid (inner shear layer). The fluctuations are thus driven more by differences in the velocity of the separate fuel and air contributions than by the turbulent mixing occurring within the fuel and air contributions. Fluctuations in regions where the velocity distributions are bimodal are not, therefore, a good indicator of turbulent mixing. A better indicator of turbulent mixing would be fluctuations in the individual peaks of the bimodal distribution. This would make the stagnation zone fluctuations more consistent with the results upstream and downstream of the stagnation zone.

E. Turbulent Kinetic Energy

From the measurements of the axial, radial, and azimuthal velocity components the turbulent kinetic energy $k = (u'^2 + v'^2 + w'^2)/2$ was determined. Figure 11 shows contour lines of constant k for $U_j/U_a = 2.8$, 1.4, and 0.84. Regions of high k occur along the initial part of the fuel-jet shear layer in all cases. In addition, for the high and medium air velocity cases, high k values are found along the centerline downstream of the fuel-jet exit and in the shear region between the outer air flow and the recirculation zone. The centerline maxima for the $U_j/U_a = 1.4$ and 0.84 cases coincide with the locations of the fuel-jet stagnation points in each flow. The values of k within the fuel-jet and annular-air shear layers are reasonable and consistent with typical shear-layer levels. However, values of k in the stagnation zones are significantly higher. Based on the conditional seeding and velocity probability distribution results, these high levels are due to large-scale boundary movement through the fixed sampling volume and smaller scale motion on either side of the boundary. Since large-scale movement in this boundary does not directly contribute to small-scale mixing, the total k value is not a good indicator of mixing in a stagnation zone. A better value of k would be based only on small-scale motions, as described earlier.

It is important to mention that prior model predictions for bluff-body flows using a k-ε model significantly underpredicted values of k in the stagnation zone.[4] This lack of agreement was seen as a major deficiency of the models and various model corrections were attempted to improve agreement. Since k is used to determine the mixing rate in these models, implicit in the observed underprediction of k is an underprediction of the mixing rate. Measurements in the present study show that the high values of k in stagnation zones are due to large-scale boundary movement, which does not directly contribute to mixing. Therefore, even if ad hoc corrections were incorporated into k-ε models to match experimental k values in the stagnation zone, reaction rates would be overpredicted since the total k is not a good indicator of mixing in these zones. Outside of the stagnation zone, measured k values are a more reasonable indicator of mixing. These observations highlight the need to apply caution when utilizing k-ε based models to pre-

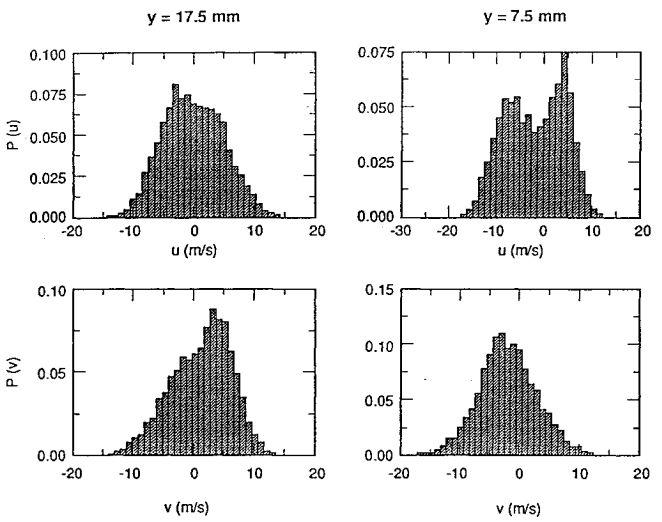

Fig. 9 Probability distributions of axial (top) and radial (bottom) velocity at x = 30 mm in a bluff-body stabilized methane jet; distributions shown correspond to the outer shear layer (y = 17.5 mm) and the central jet shear layer (y = 7.5 mm); U_j/U_a = 0.84.

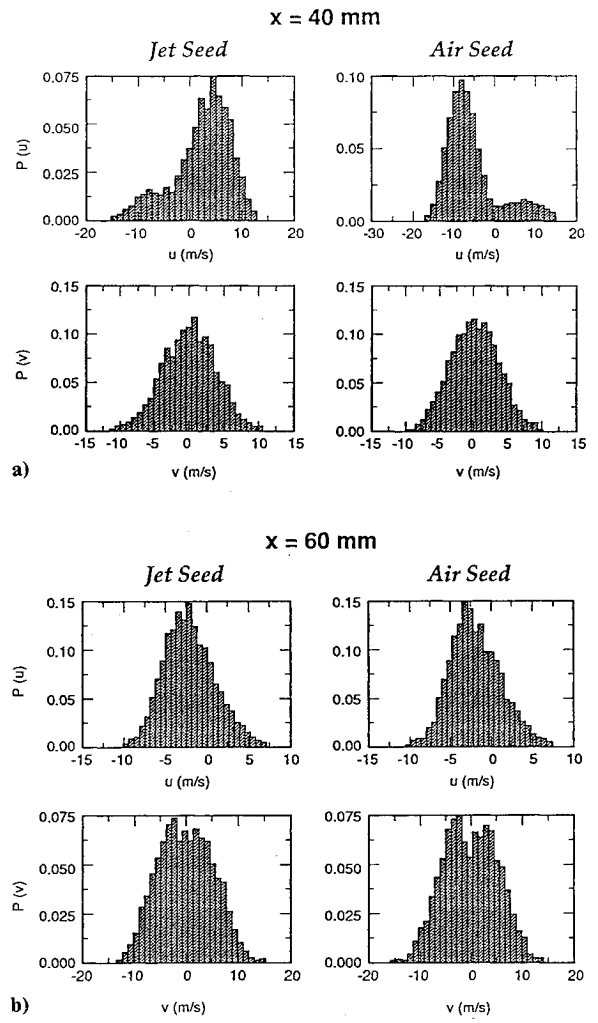

Fig. 10 Conditionally sampled probability distributions of axial (top) and radial (bottom) velocity in a bluff-body stabilized methane jet; distributions are shown along the centerline at axial locations corresponding to the fuel jet stagnation point at x = 40 mm (Fig. 11a) and to the air stagnation point at x = 60 mm (Fig. 11b); U_j/U_a = 0.84. Distribution for LDV seed added to the fuel jet is shown on the left; distribution for LDV seed added to the annular air is shown on the right.

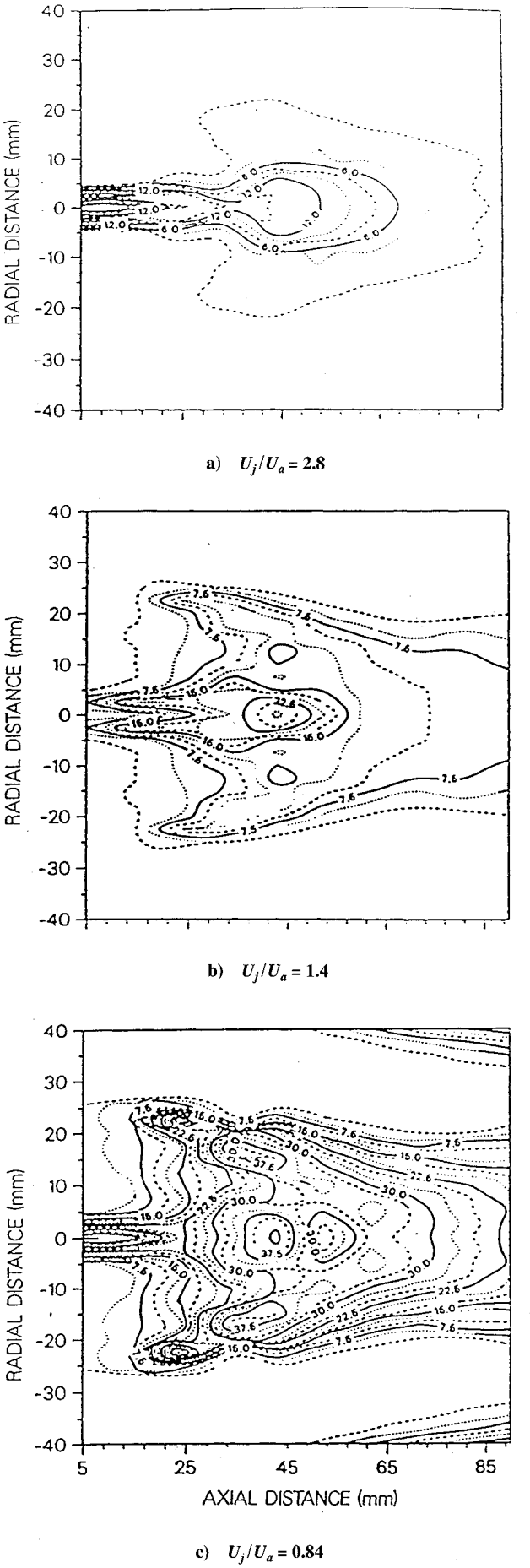

Fig. 11 Contours of turbulent kinetic energy in bluff-body stabilized methane jet.

dict turbulent combustion in flows which may have a significant large-scale time varying component.

IV. Summary and Conclusions

Velocity measurements have been obtained in a turbulent bluff-body stabilized flow. Results were obtained for three fuel-jet to outer air velocity ratios to study the effects of inlet velocity ratio on the turbulence and flowfield characteristics. At low inlet velocity ratios the flow is dominated by the reverse flow of the annular air stream and exhibits well-defined fuel jet and annular air stagnation points along the centerline. As the velocity ratio is increased, fuel-jet penetration increases until the dynamic pressure of the jet is sufficient to overcome the adverse pressure gradient of the outer air and the fuel jet penetrates the recirculation zone. Under these conditions the stagnation points move off the centerline, and the flow is best described as dominated by the fuel jet. Probability distributions of individual velocity components are bimodal in regions of high shear located along the recirculation zone boundaries and in downstream stagnation zones. Conditional seeding of the central jet and annular air shows that the two modes of the bimodal distributions are associated with the alternate passage of unmixed or partially mixed fuel and air through the measurement volume. The importance of large-scale structure and intermittency in these flows is emphasized by instantaneous Mie scattering pictures, which show a considerably different flow structure than is indicated from the time-averaged velocity field. Significant departures from isotropy are found in regions of high shear where the fluctuating axial velocity component is nearly a factor of 2 greater than the radial velocity component.

Acknowledgments

This research was supported by the United States Department of Energy, Office of Basic Energy Sciences, Division of Chemical Sciences, through Sandia National Laboratories, Livermore and by the Physical Sciences Department of the Gas Research Institute through Altex Technologies Corporation.

References

[1]Krishnamurthy, L., Wahrer, D. J., and Cochran, H. S., "Similarity Considerations of Isothermal Turbulent Recirculating Flowfields in Axisymmetric and Bluff-Body Wakes," AIAA Paper 83-1203, June 1993.

[2]Krishnamurthy, L., and Park, S. O., "Streamline Curvature Effects in Confined Isothermal Recirculating Flowfields Behind an Axisymmetric Bluff Body; Numerical Calculations with the k-ε Model," Fourth Shear Flow Symposium, Karlschruhe, Germany, 1983.

[3]Roquemore, W. M., Bradley, R. P., Stutrud, J. S., Reeves, C. M., Obringer, C. A., and Britton, R. L., "Utilization of Laser Diagnostics to Evaluate Combustion Models," AGARD-CP-353, 1983, pp. 36-1, 36-21.

[4]Correa, S. M., "Prediction of an Axisymetric Combusting Flow," *AIAA Journal,* Vol. 22, No. 11, 1984, pp. 1602–1608.

[5]Correa, S. M., and Gulati, A., "Measurements and Modeling of a Bluff-Body Stabilized Flame," *Combustion and Flame,* Vol. 89, 1992, pp. 195–213.

[6]Roquemore, W. M., Bradley, R. P., Stutrud, J. S., Reeves, C. M., Britton, R. L., Sandhu, S. A., and Archer, R. S., "Influence of the Vortex Shedding Process on a Bluff-Body Diffusion Flame," AIAA Paper 83-0335, Jan. 1983.

[7]Roquemore, W. M., Tankin, R. S., Chiu, H. H., and Lottes, A. A., "The Role of Vortex Shedding in a Bluff-Body Combustor," *Experimental Measurements and Techniques in Turbulent Reactive and Nonreactive Flows,* edited by R. M. C. So, J. H. Whitelaw, and M. Lapp, Vol. 66, American Society of Mechanical Engineers, Applied Mechanics Division, New York, 1984.

[8]Magill, P. D., Lightman, A. J., Orr, C. E., Bradley, R. P., and Roquemore, W. M., "Simultaneous Velocity and Emission Measurements in a Bluff-Body Combustor," AIAA Paper 82-0883, Jan. 1982.

[9]Namazian, M., Kelly, J., and Schefer, R. W., "Concentration Imaging Measurements in Turbulent Concentric-Jet Flows, Nonpremixed Bluff-Body Burner Flow and Flame Imaging Study," *AIAA Journal,* Vol. 30, No. 2, 1992, pp. 384–394.

[10]Schefer, R. W., Namazian M., and Kelly, J., "Velocity Measurements in a Turbulent Nonpremixed Bluff-Body Stabilized Flame," *Combustion Science Technology,* Vol. 56, 1987, pp. 101–138.

[11]Namazian, M., Kelly, J., Schefer, R. W., and Johnston, S. C., "Nonpremixed Bluff-Body Burner Flow and Flame Imaging Study," *Experimental Fluids,* Vol. 8, 1989, pp. 216–228.